JACS
JOURNAL OF THE AMERICAN CHEMICAL SOCIETY
Article
pubs.acs.org/JACS

Theoretical Study of Interfacial Electron Transfer from Reduced Anatase TiO_2(101) to Adsorbed O_2

Ye-Fei Li and Annabella Selloni*

Department of Chemistry, Princeton University, Princeton, New Jersey 08544, United States

Supporting Information

ABSTRACT: We study the electron transfer from a reduced TiO_2 surface to an approaching O_2 molecule using periodic hybrid density functional calculations. We find that the formation of an adsorbed superoxo species, $*O_2^-$, via the reaction $O_2(gas) + e^- \rightarrow *O_2^-$, is barrierless, whereas the transfer of another electron to transform the superoxo into an adsorbed peroxide, i.e. $*O_2^- + e^- \rightarrow *O_2^{2-}$, is nonadiabatic and has a barrier of 0.3 eV. The origin of this nonadiabaticity is attributed to the instability of an intermediate where the second electron is localized at the superoxo adsorption site. These results can explain the experimental finding that O_2 is not an efficient electron scavenger in photocatalysis.

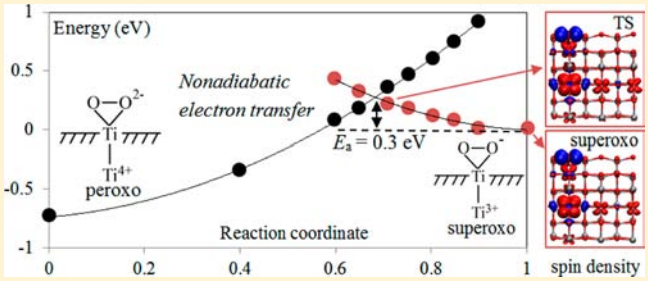

1. INTRODUCTION

TiO_2-based photocatalysis has been an area of intense research for more than 40 years.[1] A photocatalytic reaction generally includes the following steps: (i) the generation of electron−hole pairs under irradiation, (ii) the migration of photoinduced holes/electrons from the bulk to the surface, and (iii) the oxidation/reduction of adsorbates by surface-trapped holes/electrons. Among these steps, the interfacial electron transfer is believed to be essential for heterogeneous photocatalytic processes.[2] To date, extensive work has been done on the mechanisms,[3,4] yields, and selectivity[5−7] of photocatalytic reactions, but the details of the interfacial electron transfer are not yet well understood. An atomic-level understanding of this process in a prototypical photo-oxidation or reduction reaction not only would be of great scientific interest but could also help to improve the efficiency of TiO_2-based photocatalysis.

Molecular oxygen (O_2) is a clean and widely used "electron scavenger" in photo-oxidation reactions. However, kinetics experiments and calculations have shown that O_2 is not very efficient as an electron scavenger and may limit the overall photocatalytic rate.[8−13] By analyzing various mechanistic models, Gerischer et al. showed that the overall quantum efficiency of large ($R > 1$ μm) TiO_2 particles is limited not by the diffusion of O_2 but rather by the rate of electron transfer to adsorbed O_2.[13] Successively, Wang et al. provided experimental evidence that electrons accumulate on TiO_2 particles during the photocatalytic oxidation of aqueous methanol.[10] Altogether, these studies also show that the electron transfer at the TiO_2/O_2 interface plays an essential role in the whole photocatalytic redox cycle.

It is generally agreed that molecular oxygen is first reduced to a superoxo O_2^-,[2,14−16] which is the precursor of other further reduced active species, such as O_2^{2-}, O_2H^-, H_2O_2, etc.[4,17] The presence of O_2^- during O_2 reduction on TiO_2 has been identified unambiguously by EPR experiments.[14,16] On the other hand, on the basis of in situ infrared measurements, Nakamura et al. proposed the occurrence of Ti−O_2^{2-} and Ti−OOH^- species,[4] which were later confirmed by DFT calculations by Mattioli et al.[17] Although the O_2 reduction on TiO_2 has been studied for decades, the kinetics of electron transfer from TiO_2 to O_2 is still unclear.

First-principles density functional theory (DFT) calculations have proven to be a valuable tool for obtaining detailed information on photocatalytic reaction mechanisms[3,18−20] and searching for promising photocatalytic materials.[21] However, to date, theoretical studies of photocatalysis have mainly focused on thermodynamic properties, e.g. the free energy changes in the elementary steps of a reaction.[18,19] DFT studies of interfacial electron transfer in photocatalytic reactions are still relatively scarce.[22−24] This might be due to the fact that the "transition state" in an electron transfer process usually cannot be directly determined by geometrical parameters, such as bond lengths or bond and dihedral angles, but is related to the "reorganization energy",[25,26] which is difficult to calculate by DFT methods.[27] In addition, the photoinduced electron/hole involved in photocatalytic processes cannot be correctly described by local (LDA) or semilocal (GGA) exchange-correlation functionals due to the well-known delocalization error,[28] which underestimates the band gap and overdelocalizes the electron/hole states. Post-LDA/GGA functionals, e.g. hybrid functionals, are usually needed to overcome this problem. However, due to their high computational cost,

Received: April 23, 2013
Published: May 28, 2013

   dx.doi.org/10.1021/ja404044t | J. Am. Chem. Soc. 2013, 135, 9195−9199

only in recent years have hybrid functionals started to be used for the study of heterogeneous catalytic processes.[29,30]

In this paper, we investigate the interfacial electron transfer between an O_2 molecule and TiO_2 by utilizing periodic hybrid DFT calculations. Molecular oxygen interacts weakly with stoichiometric TiO_2 surfaces. In fact, O_2 adsorption occurs via interfacial electron transfer from the surface to the molecule, which is possible only when the TiO_2 surface is reduced.[2] We model the reduced surface by adding one or two excess electrons to the stoichiometric anatase (101) surface, the majority surface of the anatase TiO_2 polymorph most widely used in photocatalysis.[31] Our results provide evidence that the first electron transfer to form an adsorbed superoxo O_2^- species is barrierless, whereas the second electron transfer to form peroxo O_2^{2-} has a barrier of about 0.3 eV and a small electronic coupling energy, which makes O_2 an inefficient electron scavenger for photocatalysis.

2. METHODOLOGY AND CALCULATION DETAILS

All calculations were performed using the PBE0[32,33] hybrid functional as implemented in the CP2K/QUICKSTEP[34] package. TZV2P basis sets and Goedecker–Teter–Hutter norm-conserving pseudopotentials were used,[35] with the semicore 3s and 3p states of Ti treated explicitly. The cutoff of the real-space grid was set at 300 Ry. To model the anatase (101) surface, we used a slab with three TiO_2 layers and a rectangular surface cell with dimensions 10.398 × 11.448 Å^2, as shown in Figure 1; altogether, this corresponds to 108 atoms per unit cell.

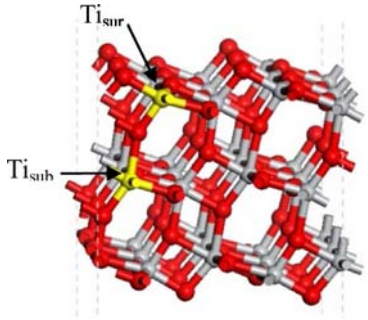

Figure 1. Anatase (101) slab model used in our calculations. Oxygens are red, and Ti atoms are gray. The two yellow spheres indicate Ti_{sur} and Ti_{sub}, the localization sites of the extra electrons which are added to describe the reduced surface.

Due to the large size of this cell, k sampling was restricted to the Γ point. The Broyden–Fletcher–Goldfarb–Shanno (BFGS) method was employed for geometry relaxations until the maximal forces on each relaxed atom were less than 0.0009 Ry/bohr. To describe the local geometrical effect caused by the excess electron, all atoms were allowed to fully relax.

In the following we investigate two-electron-transfer reactions between the reduced anatase (101) surface and molecular O_2:

$$* + O_2(g) \rightarrow *O_2^- \quad \text{(I)}$$

$$* + O_2(g) \rightarrow *O_2^{2-} \quad \text{(II)}$$

Here * denotes a Ti_{5c} adsorption site of the reduced anatase (101) surface, $O_2(g)$ represents a gas-phase molecule, and $*O_2^-$ ($*O_2^{2-}$) denotes an adsorbed superoxide (peroxide) species. The reduced surface was modeled by adding one (I) or two (II) electrons to the unit cell of the slab. In case I, the added electron was localized on a surface Ti_{5c} atom (Ti_{sur}) of the bare slab; in case II, one of the two electrons was localized on a surface Ti_{5c} atom (Ti_{sur}) and the other at a subsurface Ti_{6c} site (Ti_{sub}) (see Figure 1). The location of the added electrons was selected according to the final states of the "outward pathways" of reactions I and II discussed below.

To describe the potential energy surfaces of these reactions, we used the average Ti–O distance $d_{ads} = [d(Ti_{sur}–O_a) + d(Ti_{sur}–O_b)]/2$ as the reaction coordinate, where Ti_{sur} is the adsorption site (the same Ti_{sur} site where the electron is localized) and O_a and O_b are the two oxygen atoms in the O_2 molecule. For each reaction, we calculated two energy profiles by varying the reaction coordinate both outward, i.e from small to large d_{ads}, and inward, i.e. from large to small d_{ads}. By analyzing these two energy profiles, we can obtain a better understanding of the electron transfer process (see below). Each point on the potential energy surface was obtained using the electronic wave functions from the previous step as the initial guess, which maintains the energy profile as close as possible to the diabatic potential energy surfaces.

3. RESULTS

The energy profile of reaction I and the magnetic moments on O_2 and Ti_{sur} along the reaction coordinate are shown in parts a and b of Figure 2, respectively. Neither of these quantities

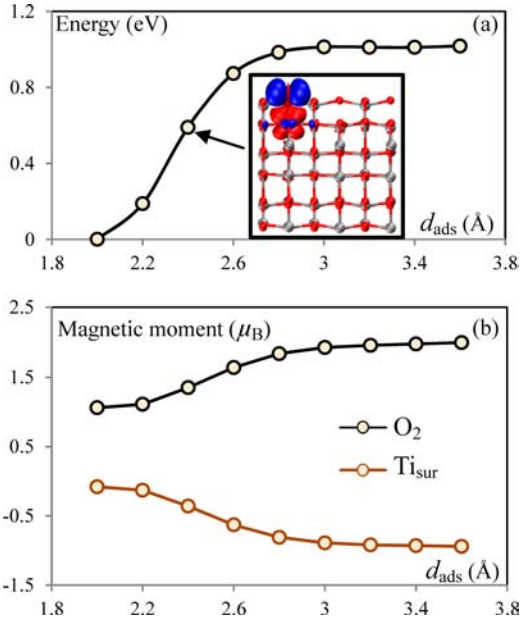

Figure 2. Potential energy profile (a) and magnetic moments (b) as a function of the average Ti–O distance (d_{ads}) for the electron transfer (I). The inset in (a) is a side view of the spin density at d_{ads} = 2.4 Å (0.001 au isosurface, with blue shown as positive and red as negative). Circles are computed values; lines are just a guide for the eye.

depends on the scan direction of the reaction coordinate, indicating that reaction I is smooth and reversible and the electron transfer process is barrierless. At a large distance from the surface, O_2 is in a triplet state with a magnetic moment of 2 μ_B (O_2 molecule) while Ti_{sur} has a magnetic moment of −1 μ_B (Ti^{3+}). Once the molecule is adsorbed as a superoxo species, its magnetic moment becomes 1 μ_B, whereas the magnetic moment of Ti_{sur} vanishes. The total magnetic moment (1 μ_B) is conserved during the electron transfer process. The spin density at d_{ads} = 2.4 Å clearly shows the electron shared between an O 2p and a Ti 3d orbital (see the inset of Figure 2a).

The computed energy profiles and magnetic moments for the two electron transfer reaction II are shown in Figure 3. At distances d_{ads} < 2.6 Å, the potential energy profile (Figure 3a) and magnetic moment (Figure 3b,c) are different for the inward

dx.doi.org/10.1021/ja404044t | J. Am. Chem. Soc. 2013, 135, 9195–9199

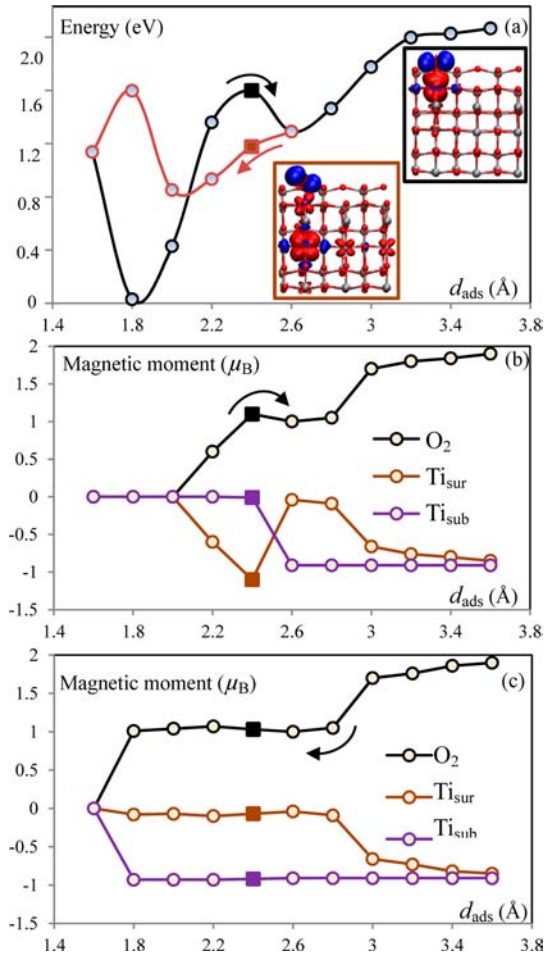

Figure 3. Energy profile (a) and magnetic moments (b and c) for reaction II. The arrow indicates the scan direction along the reaction coordinate (d_{ads}). The insets in (a) show the spin densities at d_{ads} = 2.4 Å along the inward (red box on the left) and outward (black box on the right) scan directions. The isosurface for the spin density is 0.001 au, with blue shown as positive and red as negative. Computed values are shown as circles or solid squares (at d_{ads} = 2.4 Å); the lines are just a guide for the eye.

and outward reactions. An analysis of the magnetic moments clearly shows that the reaction occurs in two steps, corresponding to the successive transfers of the two electrons. In the inward pathway, transfer of the first electron from Ti_{sur} to O_2 to form O_2^- occurs at $d_{ads} \approx 3$ Å, while the transfer of the second electron from Ti_{sub} to O_2^- to form O_2^{2-} occurs at a much shorter distance, $d_{ads} \approx 1.8$ Å. In the outward pathway, O_2^{2-} loses an electron to the surface at $d_{ads} \approx 2.4$ Å, and the superoxide O_2^- transfers again its excess electron to the surface at $d_{ads} \approx 3$ Å. Significant differences between the inward and outward pathways are present also for the spin densities, shown at d_{ads} = 2.4 Å in the inset of Figure 3a. All these results suggest the occurrence of a barrier for the transfer of an electron from TiO_2 to the adsorbed superoxide, $Ti_{sub}^{3+}-O-Ti_{sur}^{4+}<O_2^-$, to form an adsorbed peroxo species, $Ti_{sub}^{4+}-O-Ti_{sur}^{4+}<O_2^{2-}$. It is this barrier which causes the pathway to be irreversible in the range $d_{ads} \approx 1.6-2.6$ Å.

To estimate the barrier of electron transfer to $*O_2^-$, we computed the inward and outward potential energy profiles for a series of linearly interpolated geometries

$$X(\mathbf{a}) = \mathbf{a}\cdot X(\mathrm{A}) + (1 - \mathbf{a})\cdot X(\mathrm{B}) \quad (1)$$

where **a** ($0 < \mathbf{a} < 1$) is the reaction coordinate and X(A) and X(B) are the optimized geometries of $Ti_{sub}^{3+}-O-Ti_{sur}^{4+}<O_2^-$ and $Ti_{sub}^{4+}-O-Ti_{sur}^{4+}<O_2^{2-}$. As shown in Figure 4a, we found

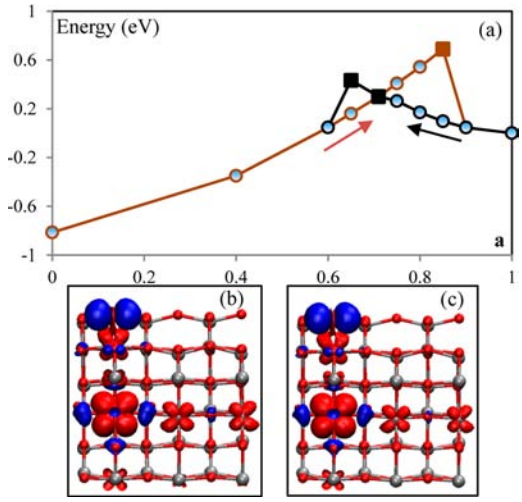

Figure 4. (a) Energy profile for the electron transfer between the superoxo $Ti_{sub}^{3+}-O-Ti_{sur}^{4+}<O_2^-$ (**a** = 1) and peroxo $Ti_{sub}^{4+}-O-Ti_{sur}^{4+}<O_2^{2-}$ (**a** = 0) states, where the reaction coordinate **a** is defined in eq 1. The arrows indicate the scan direction along **a**. (b, c) Spin densities at the transition state, **a** = 0.71, on the inward pathway (b) and at the superoxo state, **a** = 1 (c). The spin density isosurface is 0.001 au. Computed values are shown as circles or solid squares (at the transition state, **a** = 0.71, and break points, **a** = 0.65 and 0.85); lines are a guide for the eye.

a barrier of ~0.3 eV for transferring an electron to the superoxide to form a peroxide species. Furthermore, there are differences in the inward and outward pathways for $0.65 < \mathbf{a} < 0.85$, confirming that the irreversible energy profile in Figure 3 is indeed caused by the electron transfer between $Ti_{sub}^{3+}-O-Ti_{sur}^{4+}<O_2^-$ and $Ti_{sub}^{4+}-O-Ti_{sur}^{4+}<O_2^{2-}$. To estimate the influence of the supercell size on the computed barrier, we repeated the calculations after doubling the supercell size: i.e., using a (10.398×22.896 Å^2) slab with 216 atoms. The resulting barrier of 0.28 eV (see the Supporting Information) is quite consistent with the value of 0.3 eV obtained with the smaller supercell.

4. DISCUSSION AND CONCLUSIONS

At this point, it is natural to ask why the energy profile for reaction I is reversible whereas reaction II is irreversible. On the basis of Marcus theory of electron transfer,[25,26] we can understand the shape of the energy profiles in Figures 2a, 3a, and 4a in terms of the electronic coupling $H_{AB} = \langle \Psi_A | H_{el} | \Psi_B \rangle$, where Ψ_A and Ψ_B are the electronic wave functions of the reactant A and product B, respectively. H_{AB} is proportional to the electron transfer rate constant. When the coupling is strong, the electron transfer is "adiabatic", and the calculated energy profiles always follow the adiabatic potential surface. As a result, the calculated energy profiles along the two directions of the reaction coordinate are identical, as in Scheme 1a. On the other hand, if the coupling is weak, the electron transfer is "nonadiabatic", since the calculated energy profile may follow one diabatic potential surface and suddenly jump to another diabatic potential surface. We may then observe an energy profile of the type shown in Scheme 1b. The spin densities in Figures 2a, 3a, and 4b,c clearly show that the electronic

dx.doi.org/10.1021/ja404044t | J. Am. Chem. Soc. 2013, 135, 9195−9199

Scheme 1. Energy Profiles for (a) Large and (b) Small Electronic Coupling Energies

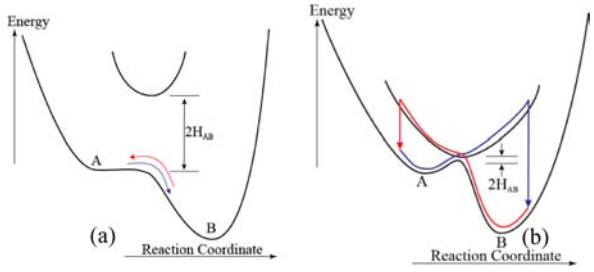

coupling energy for reaction I is large, while the electronic coupling energy for reaction II is weak. Thus, parts a and b of Scheme 1 allow us to rationalize the shape of the energy profiles shown in Figures 2a, 3a, and 4a.

To understand the origin of the small electronic coupling energy for reaction II, we further compare the spin densities of the transition state on the inward pathway (**a** = 0.71, Figure 4b) and the superoxo state (**a** = 1, Figure 4c). Interestingly, there is no significant difference between the two spin densities, indicating there is no intermediate of the type Ti_{sub}^{4+}–O–Ti_{sur}^{3+}<O_2^-, i.e. with the transferring electron localized at the Ti_{sur} site during the transfer process. There may be two reasons that prevent the electron from localizing on Ti_{sur}: (i) the electron transfer between Ti_{sub} and Ti_{sur} is difficult or (ii) the electron localization on Ti_{sur} is unstable. Analysis of the electron transfer/hopping from Ti_{sub} to Ti_{sur} in the absence of O_2 shows that this process is reversible (see Figure 5): i.e., the electronic coupling is strong. This result rules out the possibility (i) above and thus implies that Ti_{sub}^{4+}–O–Ti_{sur}^{3+}<O_2^- is unstable. To verify this conclusion, we calculated the energies of the two break points, **a** = 0.65 (inward pathway) and **a** = 0.85 (outward pathway), in Figure 4a, with the electron constrained to be localized at Ti_{sur}. The resulting energies are only ∼0.1 eV higher than those shown in Figure 4a. We infer that the inward break point at **a** = 0.65 in Figure 4a corresponds to the crossing between the diabatic potential energy surfaces for Ti_{sub}^{3+}–O–Ti_{sur}^{4+}<O_2^- and Ti_{sub}^{4+}–O–Ti_{sur}^{3+}<O_2^-, while the outward break point, **a** = 0.85, corresponds to the crossing between the diabatic potential energy surfaces for Ti_{sub}^{4+}–O–Ti_{sur}^{4+}<O_2^{2-} and Ti_{sub}^{4+}–O–Ti_{sur}^{3+}<O_2^-. This confirms that Ti_{sub}^{4+}–O–Ti_{sur}^{3+}<O_2^- is indeed unstable, which is why the electron is prevented from transferring smoothly between Ti_{sub}^{4+}–O–Ti_{sur}^{4+}<O_2^{2-} and Ti_{sub}^{3+}–O–Ti_{sur}^{4+}<O_2^-. The instability of Ti_{sub}^{4+}–O–Ti_{sur}^{3+}<O_2^- can be understood by simple covalent bond arguments. In Ti_{sub}^{4+}–O–Ti_{sur}^{4+}<O_2^{2-}, a short (∼2 Å) covalent bond forms between Ti_{sur} and O_2^-, where the bonding and antibonding states are formed mainly by the occupied 2p orbitals of O_2^- and empty 3d orbitals of Ti_{sur}, respectively. An electron added to Ti_{sur} of Ti_{sub}^{4+}–O–Ti_{sur}^{4+}<O_2^{2-} should occupy the antibonding state, which thus increases the energy of the Ti_{sub}^{4+}–O–Ti_{sur}^{3+}<O_2^- state.

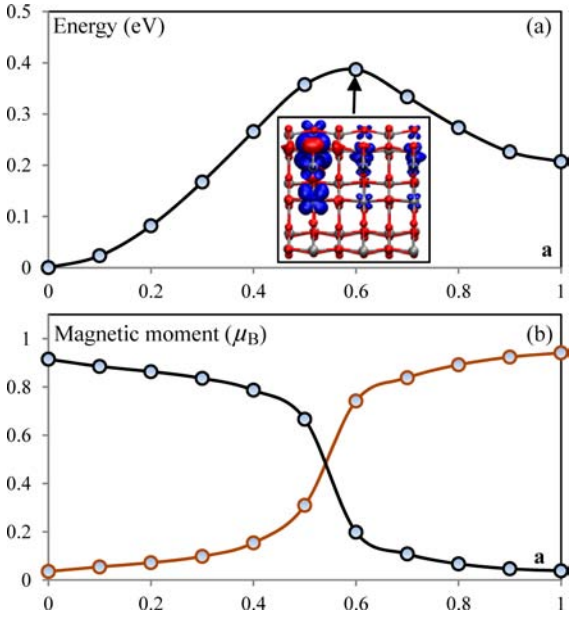

Figure 5. Energy profiles (a) and magnetic moments (b) for electron hopping between $(Ti^{3+})_{sub}$ (**a** = 0) and $(Ti^{3+})_{sur}$ (**a** = 1), obtained from linear interpolation calculations. Black and red circles in (b) refer to $(Ti^{3+})_{sub}$ and $(Ti^{3+})_{sur}$, respectively. The inset in (a) is a side view of the spin density at the transition state, **a** = 0.6 (0.001 au isosurface, with blue shown as positive and red as negative).

Another interesting question concerns the influence of oxygen vacancies and/or surface hydroxyls, which commonly exist in realistic anatase TiO_2 particles and give rise to excess electrons that tend to localize at Ti sites relatively close to the vacancy or hydroxyl.[36,37] Previous studies have shown that oxygen vacancies in anatase TiO_2 prefer to reside in the subsurface or in the bulk rather than on the surface,[38,39] and the O_2 adsorption geometry in the presence of a subsurface oxygen vacancy is similar to that without vacancy.[40] As a result, there should also exist a barrier for electron transfer between TiO_2 and O_2 due to the instability of Ti_{sub}^{4+}–O–Ti_{sur}^{3+}<O_2^-. A similar argument can be used in the case of surface hydroxyls. Still, small differences are possible between the values of the barriers for the different cases, which will require explicit calculations to be determined.

On the basis of the above analysis, we can easily understand why O_2 is not an efficient electron scavenger in photocatalytic processes. According to the mechanism proposed by Nakamura et al.,[4] the formation rate of peroxo $*O_2^{2-}$ species is directly coupled to the consumption rate of holes; therefore, the rate of $O_2(g) + 2e^- \rightarrow *O_2^{2-}$ is essential for the overall photocatalytic efficiency. Our results show that $O_2(g) + e^- \rightarrow *O_2^-$ is barrierless, while $*O_2^- + e^- \rightarrow *O_2^{2-}$ has a barrier of 0.3 eV. Furthermore, the electronic coupling energy for the latter reaction is weak, which further reduces the rate of electron transfer. There is a good deal of experimental evidence that supports the existence of a barrier for $*O_2^- + e^- \rightarrow *O_2^{2-}$. For example, EPR experiments by Komaguchi et al.[35,36] show that, on reduced rutile TiO_2, $*O_2^{2-}$ can be changed to a $*O_2^-/Ti^{3+}$ pair by visible light irradiation, which decays slowly in the dark under 77 K. Considering that $*O_2^{2-}$ is much more stable than a $*O_2^-/Ti^{3+}$ pair, the slow decay of the $*O_2^-/Ti^{3+}$ pair indicates there might exist a barrier to prevent $*O_2^-$ from transforming immediately to $*O_2^{2-}$.

In summary, this work resolves the kinetics of two successive electron transfers from TiO_2 to O_2 molecules by combining Marcus theory with periodic hybrid DFT calculations. We show that the first electron transfer to form superoxo $*O_2^-$ is barrierless, whereas the second electron transfer to form peroxo $*O_2^{2-}$ has a barrier of about 0.3 eV and is nonadiabatic, due to the instability of the Ti_{sub}^{4+}–O–Ti_{sur}^{3+}<O_2^- state. These results explain why O_2 may not be an efficient electron scavenger in photocatalysis.

dx.doi.org/10.1021/ja404044t | J. Am. Chem. Soc. 2013, 135, 9195–9199

■ ASSOCIATED CONTENT

Supporting Information

Figure giving the energy profile for electron transfer between the adsorbed superoxo and peroxo states in a (10.398 × 22.896) Å^2 supercell. This material is available free of charge via the Internet at http://pubs.acs.org.

■ AUTHOR INFORMATION

Corresponding Author

*E-mail for A.S.: aselloni@princeton.edu.

Notes

The authors declare no competing financial interest.

■ ACKNOWLEDGMENTS

This work was supported by the DoE-BES, Division of Chemical Sciences, Geosciences and Biosciences, under Award DE-FG02-12ER16286. We used resources of the National Energy Research Scientific Computing Center (DoE Contract No. DE-AC02-05CH11231). We also acknowledge use of the TIGRESS high-performance computer center at Princeton University.

■ REFERENCES

(1) Fujishima, A.; Honda, K. *Nature* **1972**, *238*, 37.
(2) Linsebigler, A. L.; Lu, G.; Yates, J. T. *Chem. Rev.* **1995**, *95*, 735.
(3) Viswanathan, V.; Hansen, H. A.; Rossmeisl, J.; Nørskov, J. K. *J. Phys. Chem. Lett.* **2012**, *3*, 2948.
(4) Nakamura, R.; Imanishi, A.; Murakoshi, K.; Nakato, Y. *J. Am. Chem. Soc.* **2003**, *125*, 7443.
(5) Zhang, M.; Wang, Q.; Chen, C.; Zang, L.; Ma, W.; Zhao, J. *Angew. Chem., Int. Ed.* **2009**, *48*, 6081.
(6) Wang, Q.; Zhang, M.; Chen, C.; Ma, W.; Zhao, J. *Angew. Chem.* **2010**, *122*, 8148.
(7) Feng, W.; Wu, G.; Li, L.; Guan, N. *Green Chem.* **2011**, *13*, 3265.
(8) Gerischer, H. *J. Phys. Chem.* **1991**, *95*, 1356.
(9) Gerischer, H. *Electrochim. Acta* **1993**, *38*, 3.
(10) Wang, C. M.; Heller, A.; Gerischer, H. *J. Am. Chem. Soc.* **1992**, *114*, 5230.
(11) Peiró, A. M.; Colombo, C.; Doyle, G.; Nelson, J.; Mills, A.; Durrant, J. R. *J. Phys. Chem. B* **2006**, *110*, 23255.
(12) Gerischer, H.; Heller, A. *J. Phys. Chem.* **1991**, *95*, 5261.
(13) Gerischer, H.; Heller, A. *J. Electrochem. Soc.* **1992**, *139*, 113.
(14) Carter, E.; Carley, A. F.; Murphy, D. M. *J. Phys. Chem. C* **2007**, *111*, 10630.
(15) Heller, A. *Acc. Chem. Res.* **1995**, *28*, 503.
(16) Wang, Z.; Ma, W.; Chen, C.; Ji, H.; Zhao, J. *Chem. Eng. J.* **2011**, *170*, 353.
(17) Mattioli, G.; Filippone, F.; Amore Bonapasta, A. *J. Am. Chem. Soc.* **2006**, *128*, 13772.
(18) Li, Y.-F.; Liu, Z.-P.; Liu, L.; Gao, W. *J. Am. Chem. Soc.* **2010**, *132*, 13008.
(19) Valdés, A.; Qu, Z. W.; Kroes, G. J.; Rossmeisl, J.; Nørskov, J. K. *J. Phys. Chem. C* **2008**, *112*, 9872.
(20) Li, Y.-F.; Liu, Z.-P. *Phys. Chem. Chem. Phys.* **2013**, *15*, 1082.
(21) García-Mota, M.; Vojvodic, A.; Metiu, H.; Man, I. C.; Su, H.-Y.; Rossmeisl, J.; Nørskov, J. K. *ChemCatChem* **2011**, *3*, 1607.
(22) Deskins, N. A.; Dupuis, M. *Phys. Rev. B* **2007**, *75*, 195212.
(23) Deskins, N. A.; Rousseau, R.; Dupuis, M. *J. Phys. Chem. C* **2010**, *114*, 5891.
(24) Deskins, N. A.; Dupuis, M. *J. Phys. Chem. C* **2008**, *113*, 346.
(25) Marcus, R. A. *J. Chem. Phys.* **1956**, *24*, 966.
(26) Marcus, R. A. *J. Chem. Phys.* **1956**, *24*, 979.
(27) Kaduk, B.; Kowalczyk, T.; Van Voorhis, T. *Chem. Rev.* **2011**, *112*, 321.
(28) Cohen, A. J.; Mori-Sánchez, P.; Yang, W. *Science* **2008**, *321*, 792.
(29) Wang, Y.; de Gironcoli, S.; Hush, N. S.; Reimers, J. R. *J. Am. Chem. Soc.* **2007**, *129*, 10402.
(30) Liu, H.-R.; Xiang, H.; Gong, X. G. *J. Chem. Phys.* **2011**, *135*, 214702.
(31) Diebold, U. *Surf. Sci. Rep.* **2003**, *48*, 53.
(32) Perdew, J. P.; Ernzerhof, M.; Burke, K. *J. Chem. Phys.* **1996**, *105*, 9982.
(33) Adamo, C.; Barone, V. *J. Chem. Phys.* **1999**, *110*, 6158.
(34) VandeVondele, J.; Krack, M.; Mohamed, F.; Parrinello, M.; Chassaing, T.; Hutter, J. *Comput. Phys. Commun.* **2005**, *167*, 103.
(35) Goedecker, S.; Teter, M.; Hutter, J. *Phys. Rev. B* **1996**, *54*, 1703.
(36) Deskins, N. A.; Rousseau, R.; Dupuis, M. *J. Phys. Chem. C* **2011**, *115*, 7562.
(37) Deskins, N. A.; Rousseau, R.; Dupuis, M. *J. Phys. Chem. C* **2009**, *113*, 14583.
(38) Cheng, H. Z.; Selloni, A. *J. Chem. Phys.* **2009**, *131*, 054703.
(39) He, Y.; Dulub, O.; Cheng, H.; Selloni, A.; Diebold, U. *Phys. Rev. Lett.* **2009**, *102*, 106105.
(40) Aschauer, U.; Chen, J.; Selloni, A. *Phys. Chem. Chem. Phys.* **2010**, *12*, 12956.